Adsorption and Diffusion of Hydrogen in a New Metal−Organic Framework Material: [Zn(bdc)(ted)$_{0.5}$]

Jinchen Liu,[†] Jeong Yong Lee,[‡] Long Pan,[‡] Richard T. Obermyer,[§] Satoru Simizu,[§] Brian Zande,[§] Jing Li,[‡] S. G. Sankar,[§] and J. Karl Johnson*[,†,||]

Department of Chemical Engineering, University of Pittsburgh, Pittsburgh, Pennsylvania 15260, Department of Chemistry & Chemical Biology, The State University of New Jersey, Piscataway, New Jersey 08854, Advanced Materials Corporation, Pittsburgh, Pennsylvania 15220, and National Energy Technology Laboratory, Pittsburgh, Pennsylvania 15236

Received: October 15, 2007; In Final Form: November 29, 2007

We have experimentally measured hydrogen isotherms at 77 and 298 K up to a hydrogen pressure of 50 bar in a recently developed metal−organic framework material, [Zn(bdc)(ted)$_{0.5}$] (bdc = benzenedicarboxylate, ted = triethylenediamine). This material has a tetragonal structure and relatively small pores. We have used atomically detailed simulations to compute adsorption isotherms of hydrogen over the same temperature and pressure ranges studied experimentally. The agreement between experiments and simulations is very good. We have included quantum effects through the Feynman−Hibbs effective potential approach; quantum effects must be included at 77 K to achieve agreement with experiments. We have used equilibrium molecular dynamics to compute self- and transport diffusivities of hydrogen in [Zn(bdc)(ted)$_{0.5}$] at both 77 and 298 K over a range of pore loadings. Quantum effects are found to decrease the self-diffusivity compared with classical simulations at fixed loading. Conversely, at fixed pressure, quantum effects lead to a lower loading and therefore a higher self-diffusion coefficient compared with classical simulation results. Transport diffusivities with and without quantum corrections are essentially indistinguishable. The diffusivities for H_2 in [Zn(bdc)(ted)$_{0.5}$] are comparable to H_2 in IRMOF-1 at 298 K.

1. Introduction

Metal-organic frameworks (MOFs) and related materials have attracted an enormous amount of attention in recent years as materials for gas sorption, gas separation and catalysis.[1−9] MOFs consist of metal vertices held together with organic linkers. They are highly crystalline and can be made inexpensively in large quantities. MOFs can be tailored fairly easily by changing metals and organic ligands. They are comparatively light, are stable over a fairly wide range of temperature and pressure, and they have uniform pore sizes, and large effective surface area and pore volume. A detailed understanding of the adsorption and diffusion properties of MOFs is important for developing applications involving membrane and pressure swing separations. While adsorption of simple gases in MOFs has been studied extensively in the past few years, there are very few studies of diffusion of gases in MOFs. Stallmach et al.[10] have studied methane, ethane, *n*-hexane, and benzene diffusion in IRMOF-1 using NMR. They found that self-diffusivities are in the range of 10^{-3}−10^{-5} cm^2/s. Atomistic simulations have been used by a few groups to study diffusion of gases in MOFs. Skoulidas[11] and Skoulidas and Sholl[12] have studied the diffusivities for Ar in MOF-2, MOF-3, IRMOF-1, and CuBTC [Cu_3-$(BTC)_2$, BTC=1,3,5- benzenetricarboxylate]. Sarkisov et al.[13] have studied the self-diffusivities of methane, *n*-pentane, *n*-hexane, *n*-heptane, cyclohexane, and benzene in IRMOF-1 at 298 K. The self-diffusivities are reported to lie in the range of 10^{-4}−10^{-5} cm^2/s. The calculated self-diffusivity of *n*-hexane is 2.2×10^{-5} cm^2/s, which agrees very well with the experimental value of 3.2×10^{-5} cm^2/s.[10] The calculated self-diffusivity of methane is about a factor of 6 lower than the value of 1.7×10^{-3} cm^2/s reported experimentally.[10] Yang and Zong[14] studied the self-diffusivities for H_2 in IRMOF-1, IRMOF-8, and IRMOF-18 at 77 K. They found self-diffusivities on the order of 10^{-4} cm^2/s, which is of the same order of magnitude as diffusion of H_2 in some zeolites. Amirjalayer et al.[15] have studied the diffusion of benzene in IRMOF-1, including the effects of lattice dynamics.

The use of MOFs as sorbents for storage of hydrogen has been studied by many groups.[4,16−18] Bhatia and Myers have studied the optimum conditions for adsorptive gas storage.[19] They found that adsorption of significant amounts of H_2 at room temperature and moderate pressure requires a heat of adsorption for H_2 of about 15 kJ/mol. It is unlikely that physisorption alone can produce a heat of adsorption this high. We therefore focus most of our study on adsorption of H_2 at 77 K, where a lower heat of adsorption will result in substantial uptake of H_2. Furthermore, Bhatia and Myers[19] pointed out that the figure of merit for a sorbent is the delivered amount of gas relative to a discharge pressure in the adsorption−desorption cycle. Following Bhatia and Myers, we use a discharge pressure of 1.5 bar to evaluate the effectiveness of materials examined in this paper.

Liu et al. have demonstrated that good agreement between experimental and simulated adsorption isotherms for simple gases in MOFs can be achieved if synthesis and activation of the MOF is carried out carefully.[20] They also showed that it is critical to account for quantum effects for simulations of H_2 at low temperatures.[20] Thus, one may expect quantitative agree-

* Author to whom correspondence should be addressed.
[†] University of Pittsburgh.
[‡] The State University of New Jersey.
[§] Advanced Materials Corporation.
[||] National Energy Technology Laboratory.

10.1021/jp710011b CCC: $40.75
Published on Web 02/02/2008

ment between simulations and experiments for gas adsorption in MOFs, if both are done carefully.

We here report experimental adsorption isotherms at 77 and 298 K for H_2 in a new MOF material, [Zn(bdc)(ted)$_{0.5}$] (bdc = benzenedicarboxylate, ted = triethylenediamine), whose synthesis has recently been reported.[21,22] We also report atomically detailed simulations of the adsorption isotherms, self-diffusivities, and transport diffusivities for H_2 adsorbed in [Zn(bdc)(ted)$_{0.5}$]. We compare our adsorption simulations with experimental data. We also compare our calculated diffusivities with simulation results for other MOFs. We assess the importance of quantum effects within our simulations for both adsorption and diffusion calculations. Finally, we compare the adsorption capacity of [Zn(bdc)(ted)$_{0.5}$] with that for CuBTC in terms of delivered adsorption amount relative to a discharged pressure of 1.5 bar.

2. Experimental Section

Instruments. Powder X-ray patterns were recorded on a Rigaku D/M-2200T automated diffractometer (Ultima+) using Cu Kα radiation (λ = 1.5406 Å). Thermal gravimetric analyses (TGA) were conducted on a TA Q50 thermogravimetric analyzer under nitrogen atmosphere (balance purge flow rate: 40.00 mL/min; sample purge flow rate: 60.00 mL/min; temperature ramping rate: 20 °C/min unless stated otherwise). Hydrogen adsorption measurements were performed on an activated (see below) sample of [Zn(bdc)(ted)$_{0.5}$] at liquid-nitrogen temperature and at room-temperature employing an apparatus built at Advanced Materials Corporation (www.advanced-material.com).

Synthesis. All chemicals used in this research were purchased from commercial providers (such as Fisher Scientific, VWR and Sigma-Aldrich) and used without further purification. The phase purity of the [Zn(bdc)(ted)$_{0.5}$] samples was confirmed by comparison of the powder X-ray diffraction patterns of the as-synthesized samples with the simulated ones from the corresponding single-crystal structures.

[Zn(bdc)(ted)$_{0.5}$]·2DMF·0.2H_2O was synthesized by solvothermal reaction of a mixture (homogenized by sonication) of zinc(II) nitrate tetrahydrate (98.5%, 1.56 g, 5.9 mmol), terephthalic acid (H_2bdc, 98%, 1.02 g, 6.0 mmol), and triethylenediamine (ted, 97%, 0.36 g, 3.1 mmol) in DMF (150 mL). The mixture was loaded in a capped glass bottle and was heated at 120 °C in an oven for 12 h. The colorless cubic crystals (2.60 g, 100% yield based on zinc nitrate tetrahydrate) were then vacuum filtered, rinsed with DMF, and dried under vacuum.

Structure Description. [Zn(bdc)(ted)$_{0.5}$]·2DMF·0.2H_2O crystallizes in a tetragonal crystal system (space group *P*4/*ncc*) with lattice constants a = 14.8999(4) Å, b = 14.8999(4) Å, c = 19.1369(2) Å.[22] It features a secondary building unit (SBU) commonly known as [$M_2C_4O_8$] paddle-wheel. Through these four-connected SBUs as nodes and the bdc ligands as linkers, a 2-dimensional (2D) net is formed. Because the bdc ligands bend significantly, the resultant 2D net is a non-symmetrical grid (Figure 1a, with a cross section of 9.2 × 5.0 Å, measured between the C atoms and calculated using van der Waals radius). The column-like triethylenediamine (ted) ligands coordinate to the metal centers from the axial directions of the paddle-wheels, giving rise to the typical pillared-layer 3D structure.[22] A structure change occurs upon removal of the guest molecules, and the crystal analysis indicated a different space group, *P*4/*mmm*.[21] Removal of the guest molecules results in a 3D porous structure containing intersecting channels of two different sizes in which all bdc ligands become straight (see Figure 1b). The larger channel is parallel to the *c* axis with a cross section 7.5 × 7.5Å

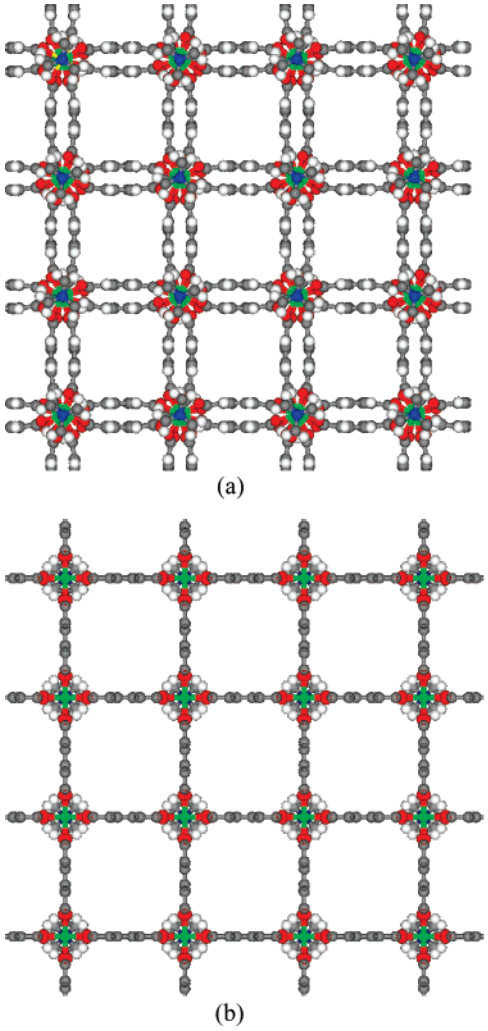

Figure 1. (a) Crystal structure of [Zn(bdc)(ted)$_{0.5}$]·2DMF·0.2H_2O viewed along *c* axis. Zn (green), O (red), C (dark gray), H (light gray), and N (blue). For clarity, guest molecules are not shown. (b) The structure after removal of guest molecules, [Zn(bdc)(ted)$_{0.5}$].[21]

(measured between the carbon atoms in the two lateral bdc ligands, taking into consideration the van der Waal's radius of carbon), and the smaller channel is along both *a*- and *b*-axes with a cross section of 4.8 × 3.2Å (measured between C−C and H−H atoms).

The pores in the material give a large free accessible volume of 61.3% (as calculated from PLATON).[23] The pores along the *c* axis can be seen in Figure 1. For comparison, note that the effective dimensions of the small and large pore diameters in CuBTC are 5 and 9 Å, respectively,[24] and the pore diameter in IRMOF-1 is 11 Å.

Adsorption Measurement. Hydrogen Pressure-Composition Isotherm (PCI) measurements were performed on a volumetric apparatus based on Sievert's principle. Prior to adsorption measurements, the [Zn(bdc)(ted)$_{0.5}$] sample was activated by heating it at ~150 °C for ~1 h to achieve an ultimate vacuum of 10^{-6} Torr using a turbo-molecular pump. About 570 mg of the sample was loaded into the sample chamber of the PCI measurement apparatus. Adsorption and desorption measurements were performed in the pressure range of 0 to ~50 bar. Additional details of the measurement technique as well as the data reduction were described in ref 20. A skeletal density of 2.54 g/cm^3 was used to determine the amount of hydrogen adsorbed under isothermal conditions. This skeletal density was derived from a pore volume of 0.73 cm^3/g measured experi-

mentally from Ar isotherm at $P/P_0 = 0.99$ and $T = 87$ K. The crystal density of 0.893 g/cm^3 was obtained from single-crystal X-ray data.

3. Computational Section

We have carried out simulations using both experimentally obtained structures shown in Figure 1, panels a and b. The atomic positions for the MOF atoms in Figure 1a were obtained from X-ray diffraction experiments described in the Supporting Information. The coordinates for the Figure 1b structure were taken from the literature.[21] The MOF atom positions were held fixed in our calculations. We have used the Lennard-Jones part of the UFF[25] potential to describe the framework atoms for the framework-fluid potentials in our simulations for adsorption and diffusion. By way of comparison, we have also used the DREIDING[26] potential for adsorption simulations. The framework potential parameters are given in Table S1 of the Supporting Information. We ignore charge-quadrupole interactions between the framework atoms and the H_2 molecule as a first approximation in our calculations. Inclusion of charge-quadrupole interactions has been shown to substantially increase the amount of H_2 adsorbed at low pressures at 77 K, while having a smaller effect at high pressures or at high temperatures.[27] We have used the Buch Lennard-Jones parameters[28] to model the H_2-H_2 interactions. The value of the diameter is $\sigma = 2.96$ Å and the potential well depth is $\epsilon/k_B = 34.2$ K, where k_B is the Boltzmann constant. The framework-fluid potentials were computed from Lorentz−Berthelot combining rules. The potentials were truncated at 17 Å without applying long-range corrections in the adsorption simulations. The diffusion calculations used a cutoff radius of 13 Å along with long-range corrections assuming a uniform density of framework atoms beyond the cutoff radius.[12] We have verified that diffusivities calculated using a cutoff radius of 13 Å with long-range corrections give results that are indistinguishable from calculations using a truncation of 17 Å without long-range corrections.

The grand canonical Monte Carlo (GCMC) method was used to calculate the adsorption isotherms.[29,30] We started from an empty MOF matrix and then performed simulations by successively increasing the fugacity. Each subsequent simulation was started from the final configuration of the previous one. Simulations were run for a total of 8×10^6 attempted moves, with half of the moves used for production data taking. A move consists of one attempt at translation, creation, or deletion of a molecule. The probability of attempting molecule creation or deletion was set to 0.3 in the simulations. An equation of state for hydrogen[31] was used to obtain the relationship between the bulk pressure and the fugacity. We have converted the total adsorption obtained from simulation to excess adsorption to compare with the experimental adsorption amount. The excess adsorption, W_{ex} (mg/g), is calculated from[27]

$$W_{ex} = \frac{1000(N_{ad} - \rho_b V_{pore,UC})M}{m_{solid,UC}} \quad (1)$$

where N_{ad} is the total number of molecules adsorbed in a unit cell, ρ_b is the bulk gas number density (molecules/cm^3), $V_{pore,UC}$ is the pore volume (free volume) in one unit cell of the MOF (cm^3), M is the molecular mass of the absorbate molecule (g/molecule), $m_{solid,UC}$ is the mass of the atoms in one unit cell of the crystal (g). We have used the pore volume of 0.73 cm^3/g measured experimentally from Ar isotherm at $P/P_0 = 0.99$ and $T = 87$ K to compute a value for $V_{pore,UC}$. This pore volume of 0.73 cm^3/g from experiments agrees very well with the value of 0.74 cm^3/g obtained from helium second virial coefficient calculations.[32] The weight percent, reported in this work, can be computed from the excess adsorption as

$$\text{wt\%} = \frac{100W_{ex}}{1000 + W_{ex}} \quad (2)$$

We have employed equilibrium molecular dynamics (EMD) simulations to compute the self- and corrected diffusivities. This same method was used previously by Skoulidas and Sholl.[12] We have performed 20−30 independent MD simulations for each loading, with a simulation length of 2−3 ns after equilibration of about 20 ps. We have calculated the transport diffusivity, which is directly related to the macroscopic flux by Fick's Law, from the following equation:

$$D_t(c) = D_0(c)\left(\frac{\partial \ln f}{\partial \ln c}\right)_T \quad (3)$$

where $D_t(c)$ is the transport diffusivity (cm^2/s), $D_0(c)$ is the corrected diffusivity (cm^2/s), f is the fugacity of the adsorbed fluid (in equilibrium with the bulk), c is the concentration of the adsorbate in the MOF, and $[(\partial \ln f)/(\partial \ln c)]_T$ is the thermodynamic correction factor, which can be calculated from adsorption isotherms obtained from GCMC simulations.

Quantum effects can be significant for H_2 at 77 K, especially at high pressures.[20] Bhatia and co-workers[33,34] have used the Feynman-Hibbs effective (FH) potential[35,36] truncated at the quartic term for the calculation of the diffusivities for H_2 and D_2 in microporous materials. Liu et al. have shown that the FH truncated at the quadratic term represents the quantum effects for the adsorption of H_2 in MOFs very well when compared with path integral Monte Carlo results at 77 K.[20] We have employed this same method to represent the quantum effects in this work for H_2 adsorption and diffusion in MOF at 77 K. We have ignored the quantum effects at room temperature since the quantum effects are small (but not zero) at 298 K.[20]

4. Results and Discussion

4.1. Comparison of Simulated H_2 Adsorption with Experiments. We have used both the classical and the FH effective Buch potentials to simulate hydrogen adsorption in [Zn(bdc)(ted)$_{0.5}$] at 77 K. We have found that the quantum corrected simulations are in better agreement with experiments than the classical simulations (see Figure S1 in the Supporting Information); this is consistent with our previous work on CuBTC.[20] We also found that adsorption isotherms computed from the two different structures in Figure 1 are in good agreement (see Figure S2 in the Supporting Information), leading us to conclude that small changes in the structure do not result in significant changes in adsorption. We therefore present only results using the structure from Figure 1a in the remainder of this paper. The FH effective potential simulation results are plotted along with experiments in Figure 2. Simulations agree very well with experiments over the entire range of pressure. The UFF force field gives slightly better agreement, as can be seen in Figure 2. Both experimental and FH effective potential simulated isotherms reach a maximum at around 20 bar and then slightly decrease with increasing pressure, as expected for excess adsorption. The low-pressure region is shown in Figure 3. There is apparently a slight hysteresis in experimental adsorption and desorption isotherms taken from the PCI apparatus at low pressure (Figure 3). We believe the hysteresis to be an artifact of the experiments; the PCI instrument is designed for high pressure measurements, so slight errors at low pressures are to

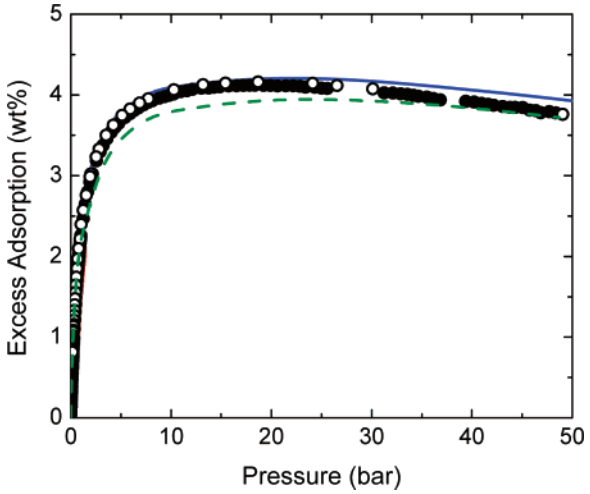

Figure 2. Comparison of simulated and experimental H_2 adsorption isotherms in [Zn(bdc)(ted)$_{0.5}$] at 77 K. The experimental results are represented by filled (open) circles for adsorption (desorption). The simulation results using FH effective Buch potential are represented by the solid line (blue) and the dashed line (olive) for the UFF and DREIDING force fields, respectively.

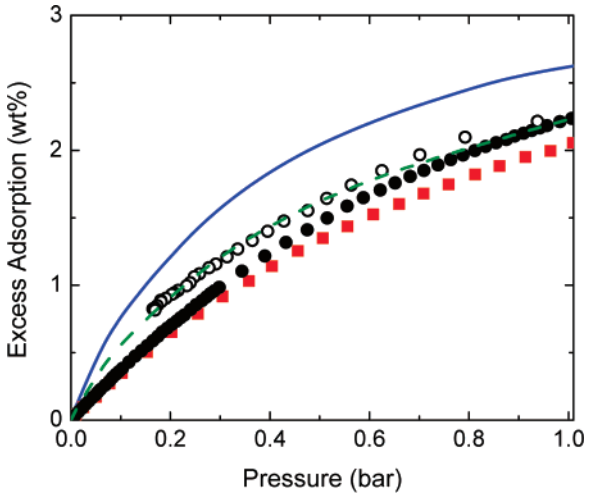

Figure 3. Comparison of simulated and experimental H_2 adsorption isotherms in [Zn(bdc)(ted)$_{0.5}$] at 77 K for the low-pressure region. The experimental results are represented by filled (open) circles for adsorption (desorption). The experimental data from Lee et al.[22] are shown as filled squares. The simulation results using FH effective Buch potential are represented by the solid line (blue) and the dashed line (olive) for the UFF and DREIDING force fields, respectively.

be expected. Hence, the agreement between our experimental results and the experimental data by Lee et al.[22] is acceptable. Simulations using the DREIDING force field agree very well with our experiments at low pressure (Figure 3) but underpredict the amount adsorbed at high pressure (Figure 2). In contrast, simulations using UFF significantly overpredict the adsorption at low pressures and slightly overpredict the adsorption at high pressures. We observe that the experimental data above a pressure of about 1 bar lie in between the predictions from the UFF and DREIDING force fields, indicating that the small discrepancy between simulations and experiments above 1 bar is likely due to errors in the solid-fluid potential. The overall good agreement between simulations and experiments indicates that the [Zn(bdc)(ted)$_{0.5}$] sample is of high purity and that guest molecules (solvents) were effectively removed.

We have also compared the simulation results at room temperature with experiments, shown in Figure 4. Simulations using the DREIDING potential agree very well with experiments, and simulations using UFF force field overestimate experiments. The largest error between simulations and experiments is about 0.07 (0.02) wt% for the UFF (DREIDING) force field. The agreement between simulations and experiments is acceptable, considering that the estimated error in experiments is about 0.04 wt % at the highest pressure (50 bar). Note that we only employ the classical potential at room temperature. Using the FH effective potential at room temperature is known to overcorrect for quantum effects.[20]

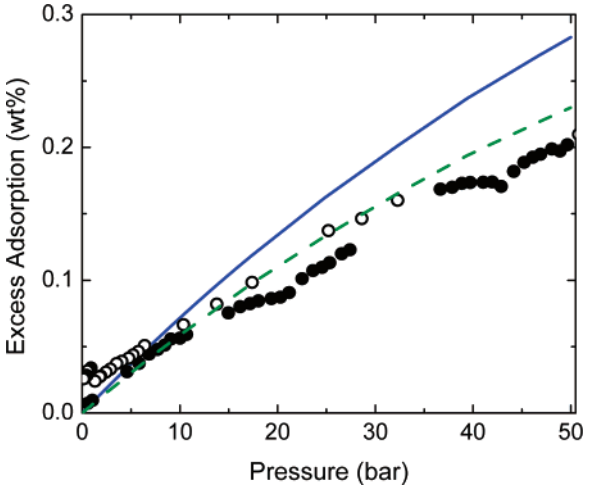

Figure 4. Comparison of simulated and experimental H_2 adsorption isotherms in [Zn(bdc)(ted)$_{0.5}$] at 298 K. The experimental results are represented by filled (open) circles for adsorption (desorption). The simulation results using Buch potential are represented by the solid line (blue) and the dashed line (olive) for the UFF and DREIDING force fields, respectively.

There are two practical metrics of efficiency for a microporous adsorbent: (1) the capacity of the material to adsorb H_2 with respect to an empty container and (2) amount of H_2 that can be delivered relative to a discharge pressure in an adsorption−desorption cycle, with the latter property being more important.[19] We have calculated the excess adsorption with respect to an empty container and the delivered amount of H_2 relative to a discharge pressure of 1.5 bar for [Zn(bdc)(ted)$_{0.5}$] and have compared with these quantities for CuBTC (see Figure 5). These quantities are calculated from the total amount of adsorbed, rather than the excess adsorption. We show the total adsorption for these two materials in Figure 5 for comparison. The total adsorption of H_2 in [Zn(bdc)(ted)$_{0.5}$] increases very abruptly with pressure, according to the simulations (the experimental data do not show such a steep uptake with increasing pressure). The amount adsorbed reaches 90% of the total capacity at a pressure of ∼24 bar for [Zn(bdc)(ted)$_{0.5}$] compared with a higher pressure of ∼40 bar for CuBTC. This is due to the pores in [Zn(bdc)(ted)$_{0.5}$] being much smaller than those of CuBTC. The effective pore size is 7.5 × 7.5 Å in the z direction (along c axes) and 4.8 × 3.2 Å in the x and y directions (see Figure 1) for [Zn(bdc)(ted)$_{0.5}$]. This corresponds to a maximum capacity of 2−3 and 1−2 layers of H_2 molecules adsorbed in the large and small pores, respectively. Small pores display a steep rise in the amount adsorbed with increasing pressure because of the strong solid-fluid interaction potential. Moreover, the pores in [Zn(bdc)(ted)$_{0.5}$] are relatively uniform, which also contributes to the steep rise in the amount adsorbed at low pressure. The existence of small and large pores of about 5 and 9 Å in diameter for CuBTC leads to a more gradual increase in the adsorption isotherm with increasing pressure. However, the adsorption capacity for these two materials at highest pressure is very similar owing to their similar pore

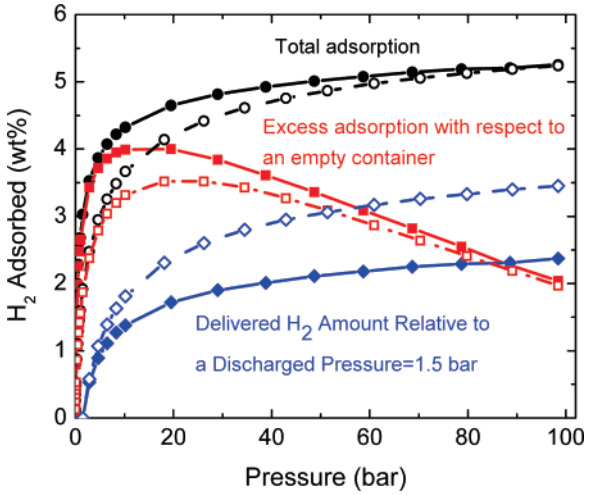

Figure 5. Comparison of simulated H_2 adsorption isotherms in [Zn(bdc)(ted)$_{0.5}$] (solid symbols) and CuBTC (open symbols) at 77 K using FH effective Buch potential. The total adsorption, the excess adsorption with respect to an empty container, and the delivered H_2 amount relative to a discharge pressure of 1.5 bar are represented by circles, squares, and diamonds, respectively. The adsorption isotherm for CuBTC is taken from Liu et al.[20] The lines are to guide the eye.

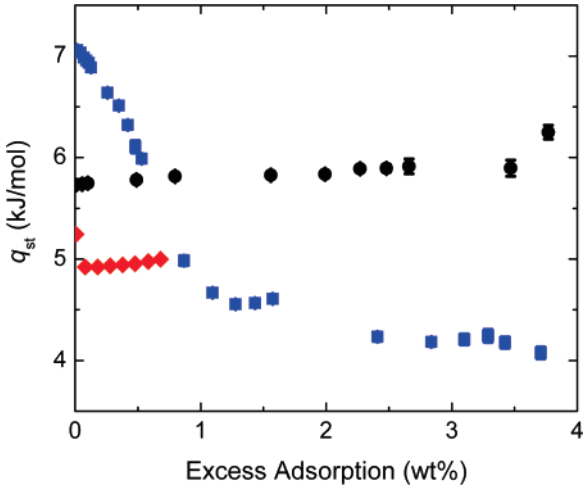

Figure 6. Comparison of the isosteric heat of adsorption for H_2 adsorption in [Zn(bdc)(ted)$_{0.5}$] and CuBTC at 77 K. The heats of adsorption from experiments[22] and simulations for [Zn(bdc)(ted)$_{0.5}$] are represented by diamonds and circles, respectively. The heats of adsorption from simulations for CuBTC are represented by squares.

volumes. The excess adsorption with respect to an empty container for [Zn(bdc)(ted)$_{0.5}$] is larger than that for CuBTC at low pressures, as expected from the total adsorption isotherms. The maximum value is reached at about 10 and 18 bar for [Zn(bdc)(ted)$_{0.5}$] and CuBTC, respectively. For the delivered H_2 amount relative to a discharged pressure of 1.5 bar, [Zn(bdc)(ted)$_{0.5}$] gives smaller values than CuBTC, in contrast to the total adsorption. The difference is about 1 wt % for $P > 40$ bar. The amount of H_2 adsorbed at the discharged pressure of 1.5 bar calculated from simulations for [Zn(bdc)(ted)$_{0.5}$] is about 1.1 wt % larger than CuBTC, which means that about 1.1 wt % of H_2 in [Zn(bdc)(ted)$_{0.5}$] cannot be released in the adsorption−desorption swing compared with CuBTC. The large amount of H_2 adsorbed at the discharged pressure in [Zn(bdc)(ted)$_{0.5}$] results in its poorer performance as a H_2 storage material compared to CuBTC at 77 K in terms of delivered hydrogen. Hence, the adsorption amount at the discharge pressure is a key property to consider when evaluating hydrogen storage materials. We should mention that the above analysis is based on the simulation results, which overestimate the adsorption at the discharge pressure for [Zn(bdc)(ted)$_{0.5}$] compared with experiments. Thus, the difference in experimental results should be less than 1 wt % for these two materials.

The simulated isosteric heats of adsorption for H_2 adsorbed in [Zn(bdc)(ted)$_{0.5}$] and CuBTC at 77 K are plotted in Figure 6. Both sets of simulations used the UFF force field for the MOF, along with the FH effective Buch potential. We have also plotted the experimental heat of adsorption for H_2 in [Zn(bdc)(ted)$_{0.5}$] measured by Lee et al.[22] The simulated heat of adsorption is about 0.7 kJ/mol larger than experiments; this is consistent with the observation in Figure 3 that the amount of H_2 adsorbed at low pressure is overestimated by UFF force field compared with experiments. The heat of adsorption is nearly independent of loading for [Zn(bdc)(ted)$_{0.5}$] from both experiments and simulations. This is a result of the pores being uniform and small in [Zn(bdc)(ted)$_{0.5}$]. In contrast, the heat of adsorption is high at low coverages and decreases abruptly with increasing loading for CuBTC. The initial high heat of adsorption for CuBTC is due to the high energy adsorption sites close to metal-oxide in the small pores. The low heat of adsorption at high loading marks the adsorption of H_2 in the large pores.

4.2. Diffusivities of H_2 in [Zn(bdc)(ted)$_{0.5}$]. We have used both the classical and the FH effective Buch potentials along with the UFF force field to calculate the diffusivities for H_2 in [Zn(bdc)(ted)$_{0.5}$] at 77 K. The inclusion of quantum effects increases the self-diffusivity at zero loading and decreases the self-diffusivity at high loadings for H_2 in [Zn(bdc)(ted)$_{0.5}$], as can be seen in Figure 7a. There are two competing factors that contribute to self-diffusivity when quantum effects are considered. The first is the decrease in the diffusion energy barrier due to a nonuniform smearing of the solid-fluid potential within the Feynman-Hibbs formalism. This leads to an increase of the diffusivities. The second effect is the increase in the effective size parameter for the solid-fluid and fluid−fluid interactions. This may lead to steric hindrance in narrow pores or in larger pores at high loadings that decreases the diffusivity. At zero loading, the first factor is dominant and the self-diffusivity is increased. At high loadings, steric hindrance becomes more apparent and the self-diffusivity is decreased. Bhatia and coworkers[33,34] have found that quantum effects are very sensitive to pore dimensions for H_2 and D_2. In zeolite rho the diffusivities decrease compared with results from classical simulations. Our results at high loadings agree with these conclusions. We have plotted the self-diffusivity as a function of the bulk gas pressure in Figure 7b. Interestingly, the inclusion of quantum effects increases the self-diffusivity at fixed pressure over the entire range of pressures. The reason for this is that for a given pressure the quantum fluid amount adsorbed is significantly less than for the classical fluid. (see Figure S1) Moreover, the self-diffusivity decreases dramatically with increased loading, so that the diffusivity of the quantum fluid is larger than that of the classical fluid because the loading is so much lower.

We have calculated the self-diffusivity for the classical H_2 potential using the structure of Dybtsev et al. (see Figure S3 in the Supporting Information). The self-diffusivities in the two different structures of [Zn(bdc)(ted)$_{0.5}$] are essentially identical for low loadings and are slightly larger in the structure of Dybtsev et al.[21] at high loadings.

The transport diffusivities for H_2 in [Zn(bdc)(ted)$_{0.5}$] at 77 K are plotted in Figure 8. The quantum effects are small compared with the uncertainty and scatter in the data. In general, the transport diffusivities increase as the pressure is increased. The transport diffusivity increases by about a factor of 5 over the pressure range from zero to 60 bar.

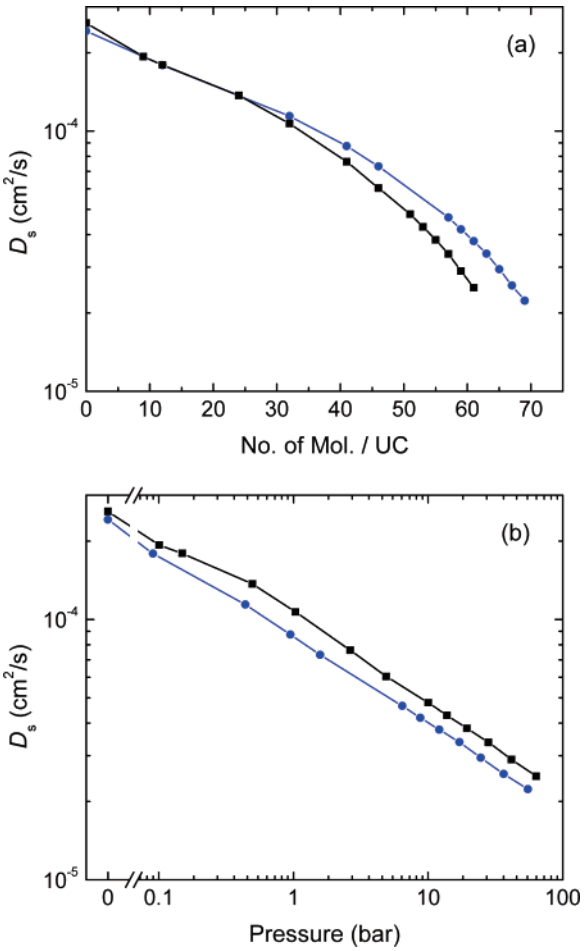

Figure 7. Self-diffusivities of H_2 in [Zn(bdc)(ted)$_{0.5}$] at 77 K. The results using classical Buch potential and FH effective Buch potential are represented by circles and squares, respectively. The lines are a guide to the eye. (a) In terms of loading. (b) In terms of the bulk gas pressure.

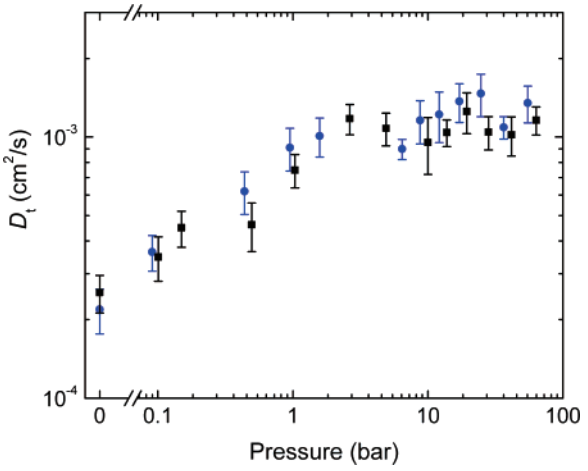

Figure 8. Transport diffusivities of H_2 in [Zn(bdc)(ted)$_{0.5}$] at 77 K. The results using the classical Buch potential and the FH effective Buch potential are represented by circles and squares, respectively.

The self- and transport diffusivities of H_2 in [Zn(bdc)(ted)$_{0.5}$] at 298 K are shown in Figure 9. Similar to the cases at 77 K, the self-diffusivities decrease with increasing pressure, and transport diffusivities increase with increasing pressure. This phenomenon is similar to H_2 diffusion in IRMOF-1 at 298 K[12] and for diffusivities in many other nanoporous materials.[37−41]

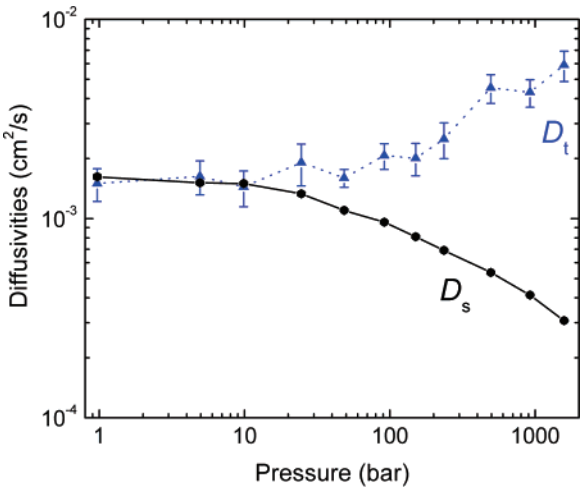

Figure 9. Self- and transport diffusivities of H_2 in [Zn(bdc)(ted)$_{0.5}$] at 298 K. D_s and D_t are represented by circles and triangles, respectively. The lines are a guide to the eye.

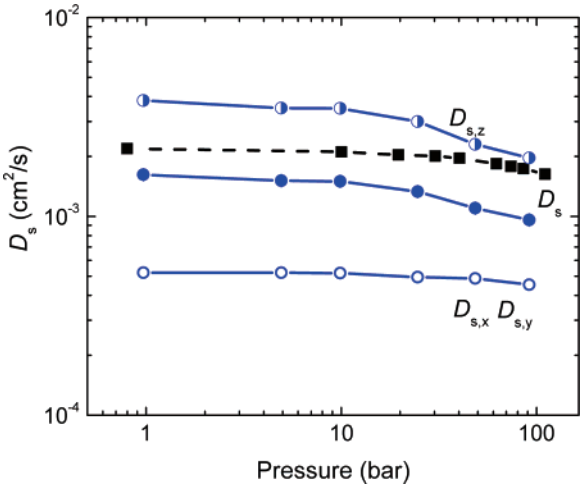

Figure 10. Self-diffusivities of H_2 in [Zn(bdc)(ted)$_{0.5}$] from our calculations and in IRMOF-1 calculated by Skoulidas and Sholl,[12] both at 298 K. The results for D_s in [Zn(bdc)(ted)$_{0.5}$] in the x and y directions are given by open circles. D_s in the z direction is given by half filled circles and the average D_s is given as solid circles. Note that $D_{s,x} = D_{s,y}$ and $D_s = (D_{s,x} + D_{s,y} + D_{s,z})/3$. The solid squares are the results for IRMOF-1.[12] The lines are a guide to the eye.

We have compared the diffusivities of H_2 in [Zn(bdc)(ted)$_{0.5}$] with those in IRMOF-1[12] at 298 K, shown in Figure 10. The self- and transport diffusivities in these two materials have the same trend (see Figure S6 for D_t). However, the diffusivities in [Zn(bdc)(ted)$_{0.5}$] are about a factor of 2 smaller than in IRMOF-1. The diffusivities in x, y, and z directions are identical in IRMOF-1 due to the uniform 3-D pores with an effective size of ~11 × 11 Å. In contrast, the pores in [Zn(bdc)(ted)$_{0.5}$] are nonuniform. The effective pore size is 7.5 × 7.5 Å in the z direction (along c axes) and 4.8 × 3.2 Å in the x and y directions. The diffusivities in z direction are about 4−8 times larger than those in x and y directions, as can be seen in Figure 10. The diffusivities for H_2 in the z direction in [Zn(bdc)(ted)$_{0.5}$] are about the same as in IRMOF-1.

5. Conclusions

We have presented experimental and simulated adsorption isotherms for H_2 in [Zn(bdc)(ted)$_{0.5}$] at 77 and 298 K. We observe good agreement between simulations and experiments, indicating that the synthesis and activation procedures success-

fully produce nearly defect and solvent free crystals. We note that small perturbations in the crystal structure give rise to minor differences in the calculated adsorption isotherms and diffusivities. The [Zn(bdc)(ted)$_{0.5}$] displays a steep increase in the amount adsorbed with pressure at 77 K. This makes [Zn(bdc)-(ted)$_{0.5}$] less attractive as a practical hydrogen storage material based on the amount of delivered hydrogen at a discharge pressure of 1.5 bar. Thus, a useful hydrogen storage material must not have too steep an isotherm at low pressures. We have calculated the self- and transport diffusivities at 77 and 298 K for H_2 in [Zn(bdc)(ted)$_{0.5}$]. Quantum effects are seen to increase the self-diffusivity at low loadings, but decrease the self-diffusivity at high loadings. In contrast, when plotted as a function of pressure rather than as a function of loading, quantum effects always increase the self-diffusivity. Transport diffusivities are not strongly influenced by quantum effects at 77 K. The diffusion properties for H_2 in [Zn(bdc)(ted)$_{0.5}$] are comparable to those of H_2 in IRMOF-1 at 298 K. Thus adsorption processes should not be diffusion-limited.

Acknowledgment. We gratefully acknowledge financial support from the National Energy Technology Laboratory (Grant # DE-FC26-05NT42446).

Supporting Information Available: Results of X-ray diffraction experiments. This material is available free of charge via the Internet at http://pubs.acs.org.

References and Notes

(1) Eddaoudi, M.; Kim, J.; Rosi, N.; Vodak, D.; Wachter, J.; O'Keefe, M.; Yaghi, O. M. *Science* **2002**, *295*, 469.
(2) Yaghi, O. M.; O'Keeffe, M.; Ockwig, N. W.; Chae, H. K.; Eddaoudi, M.; Kim, J. *Nature* **2003**, *423*, 705.
(3) Pan, L.; Adams, K. M.; Hernandez, H. E.; Wang, X. T.; Zheng, C.; Hattori, Y.; Kaneko, K. *J. Am. Chem. Soc.* **2003**, *125*, 3062.
(4) Rosi, N. L.; Eckert, J.; Eddaoudi, M.; Vodak, D. T.; Kim, J.; O'Keeffe, M.; Yaghi, O. M. *Science* **2003**, *300*, 1127.
(5) Hermes, S.; Schroter, M. K.; Schmid, R.; Khodeir, L.; Muhler, M.; Tissler, A.; Fischer, R. W.; Fischer, R. A. *Angew. Chem. Int. Ed.* **2005**, *44*, 6237.
(6) Rowsell, J. L. C.; Yaghi, O. M. *J. Am. Chem. Soc.* **2006**, *128*, 1304.
(7) Mueller, U.; Schubert, M.; Teich, F.; Puetter, H.; Schierle-Arndt, K.; Pastre, J. *J. Mater. Chem.* **2006**, *16*, 626.
(8) Pan, L.; Olson, D. H.; Ciemnolonski, L. R.; Heddy, R.; Li, J. *Angew. Chem. Int. Ed.* **2006**, *45*, 616.
(9) Pan, L.; Parker, B.; Huang, X. Y.; Olson, D. H.; Lee, J. Y.; Li, J. *J. Am. Chem. Soc.* **2006**, *128*, 4180.
(10) Stallmach, F.; Groger, S.; Kunzel, V.; Karger, J.; Yaghi, O. M.; Hesse, M.; Muller, U. *Angew. Chem. Int. Ed.* **2006**, *45*, 2123.
(11) Skoulidas, A. I. *J. Am. Chem. Soc.* **2004**, *126*, 1356.
(12) Skoulidas, A. I.; Sholl, D. S. *J. Phys. Chem. B* **2005**, *109*, 15760.
(13) Sarkisov, L.; Duren, T.; Snurr, R. Q. *Mol. Phys.* **2004**, *102*, 211.
(14) Yang, Q. Y.; Zhong, C. L. *J. Phys. Chem. B* **2005**, *109*, 11862.
(15) Amirjalayer, S.; Tafipolsky, M.; Schmid, R. *Angew. Chem. Int. Ed.* **2007**, *46*, 463.
(16) Dietzel, P. D. C.; Panella, B.; Hirscher, M.; Blom, R.; Fjellvag, H. *Chem. Commun.* **2006**, *9*, 959.
(17) Pan, L.; Sander, M. B.; Huang, X. Y.; Li, J.; Smith, M.; Bittner, E.; Bockrath, B.; Johnson, J. K. *J. Am. Chem. Soc.* **2004**, *126*, 1308.
(18) Zhao, X. B.; Xiao, B.; Fletcher, A. J.; Thomas, K. M.; Bradshaw, D.; Rosseinsky, M. J. *Science* **2006**, *306*, 1012.
(19) Bhatia, S. K.; Myers, A. L. *Langmuir* **2006**, *22*, 1688.
(20) Liu, J.-C.; Culp, J. T.; Natesakhawat, S.; Bockrath, B. C.; Zande, B.; Sankar, S. G.; Garberoglio, G.; Johnson, J. K. *J. Phys. Chem. C* **2007**, *111*, 9305.
(21) Dybtsev, D. N.; Chun, H.; Kim, K. *Angew. Chem. Int. Ed.* **2004**, *43*, 5033.
(22) Lee, J. Y.; Olson, D. H.; Pan, L.; Emge, T. J.; Li, J. *Adv. Func. Mater.* **2007**, *17*, 1255.
(23) Spek, A. L. *J. Appl. Crystallogr.* **2003**, *36*, 7.
(24) Vishnyakov, A.; Ravikovitch, P. I.; Neimark, A. V.; Bulow, M. *Nano Lett.* **2003**, *3*, 713.
(25) Rappe, A. K.; Casewit, C. J.; Colwell, K. S.; Goddard, W. A.; Skiff, W. M. *J. Am. Chem. Soc.* **1992**, *114*, 10024.
(26) Mayo, S. L.; Olafson, B. D.; Gaddard, W. A., III. *J. Phys. Chem.* **1990**, *94*, 8897.
(27) Garberoglio, G.; Skoulidas, A. I.; Johnson, J. K. *J. Phys. Chem. B* **2005**, *109*, 13094.
(28) Buch, V. *J. Chem. Phys.* **1994**, *100*, 7610.
(29) Allen, M. P.; Tildesley, D. J. *Computer Simulation of Liquids*; Oxford University Press: New York, 1987.
(30) Frenkel, D.; Smit, B. *Understanding Molecular Simulation: From Algorithms to Applications*; Academic Press: London, 1996.
(31) Younglove, B. A. *J. Phys. Chem. Ref. Data Suppl.* **1982**, *11*, 1.
(32) Myers, A. L.; Monson, P. A. *Langmuir* **2002**, *18*, 10261.
(33) Kumar, A. V. A.; Bhatia, S. K. *Phys. Rev. Lett.* **2005**, *95*, 245901.
(34) Kumar, A. V. A.; Jobic, H.; Bhatia, S. K. *J. Phys. Chem. B* **2006**, *110*, 16666.
(35) Feynman, R. P. *Statistical Mechanics; A Set of Lectures*; W. A. Benjamin: Reading, MA, 1972.
(36) Feynman, R. P.; Hibbs, A. R. *Quantum Mechanics and Path Integrals*; McGraw-Hill: New York, 1965.
(37) Skoulidas, A. I.; Sholl, D. S. *J. Phys. Chem. B* **2001**, *105*, 3151.
(38) Skoulidas, A. I.; Sholl, D. S. *J. Phys. Chem. B* **2002**, *106*, 5058.
(39) Skoulidas, A. I.; Ackerman, D. M.; Johnson, J. K.; Sholl, D. S. *Phys. Rev. Lett.* **2002**, *89*, 185901.
(40) Ackerman, D. M.; Skoulidas, A. I.; Sholl, D. S.; Johnson, J. K. *Mol. Simul.* **2003**, *29*, 677.
(41) Skoulidas, A. I.; Sholl, D. S.; Johnson, J. K. *J. Chem. Phys.* **2006**, *124*, 054708.